Supplementary Material

OA concentrations and source contribution at BCN and MSY sites using a local bottom-up emission inventory

Figure S1 shows the time series of OA concentrations and source contributions for BCN and MSY sites derived from a simulation of the MONARCH model using a local bottom-up emission inventory for Spain (HERMESV3_BU Guevara et al., 2020). The simulation was conducted for the months of January and July with a spatial resolution of $\sim$ 5 km. Main differences between HERMESv3_BU and CAMS-REG_v4.2 inventories are discussed in Navarro-Barboza et al. (2024). In contrast to results using the CAMS inventory depicted in Figure 4, results with the HERMESv3_BU inventory closely align with observational data in BCN and MSY, particularly during winter. The comparison between the two inventories reveals marked differences in OA component contributions. For instance, with HERMESv3_BU, the residential component is less dominant than with CAMS, and the traffic component becomes more significant. A similar pattern is observed in MSY, where the CAMS inventory results tend to overestimate winter concentrations due to the residential component. These discrepancies highlight the existing constraints of European-scale emission inventories, even though they remain the most reliable information source at present.

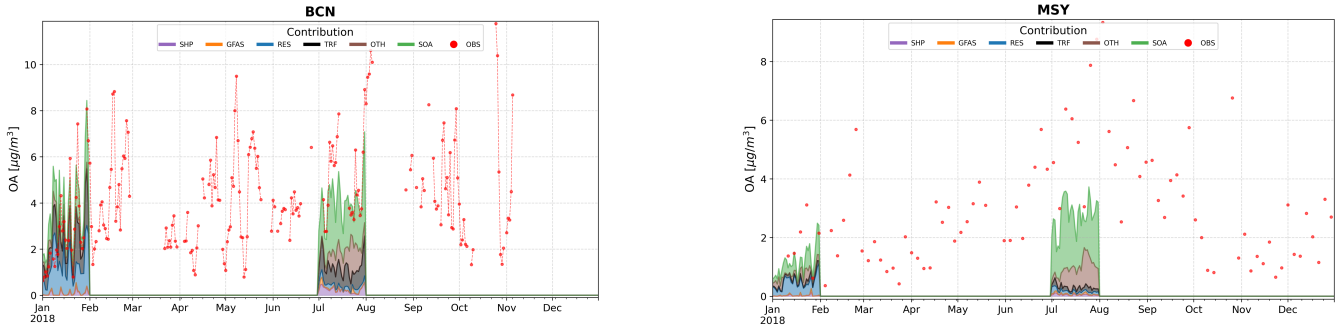

(a) (b)

Figure S1. Daily average contributions of OA concentration in BCN (a) and MSY (b) for the year 2018, using the local bottom-up HERMESv3 emission inventory. Measurements are expressed in [$\mu\ gm^{-3}$], with each component distinguished by a specific color: Shipping (SHIP) in purple, Fires (GFAS) in orange, Residential (RESI) in blue, Traffic (TRAF) in black, Other (OTHR) in brown, and Secondary OA (SOA) in green. Observational data (OBS) are marked with red dots. Due to the limitations in simulation data availability, only the months of January and July are depicted.

Seasonal Comparison of Modeled vs. Observed OA Concentrations Across Europe

Figure S2 presents scatter plots comparing modeled and observed OA concentrations across twelve stations. The correlation coefficients (r) vary by site, ranging from 0.21 at MSY to 0.77 at PAY, indicating different levels of agreement between the model and observations. At the KRA and DEM stations, the model tends to overestimate OA concentrations, as indicated by positive fractional bias (FB) values of 32.17 and 34.57, respectively. Conversely, at the HEL and MSY stations, the model underestimates OA concentrations, with negative FB values of -19.31 and -37.90, respectively. Seasonal variations are evident in the scatter plots. Higher concentrations are observed during the DJF (blue) and MAM (orange) seasons, particularly at KRA and RIG, while lower concentrations are seen during the JJA (green) and SON (red) seasons. This seasonal trend highlights the importance of considering temporal variations in OA modeling.

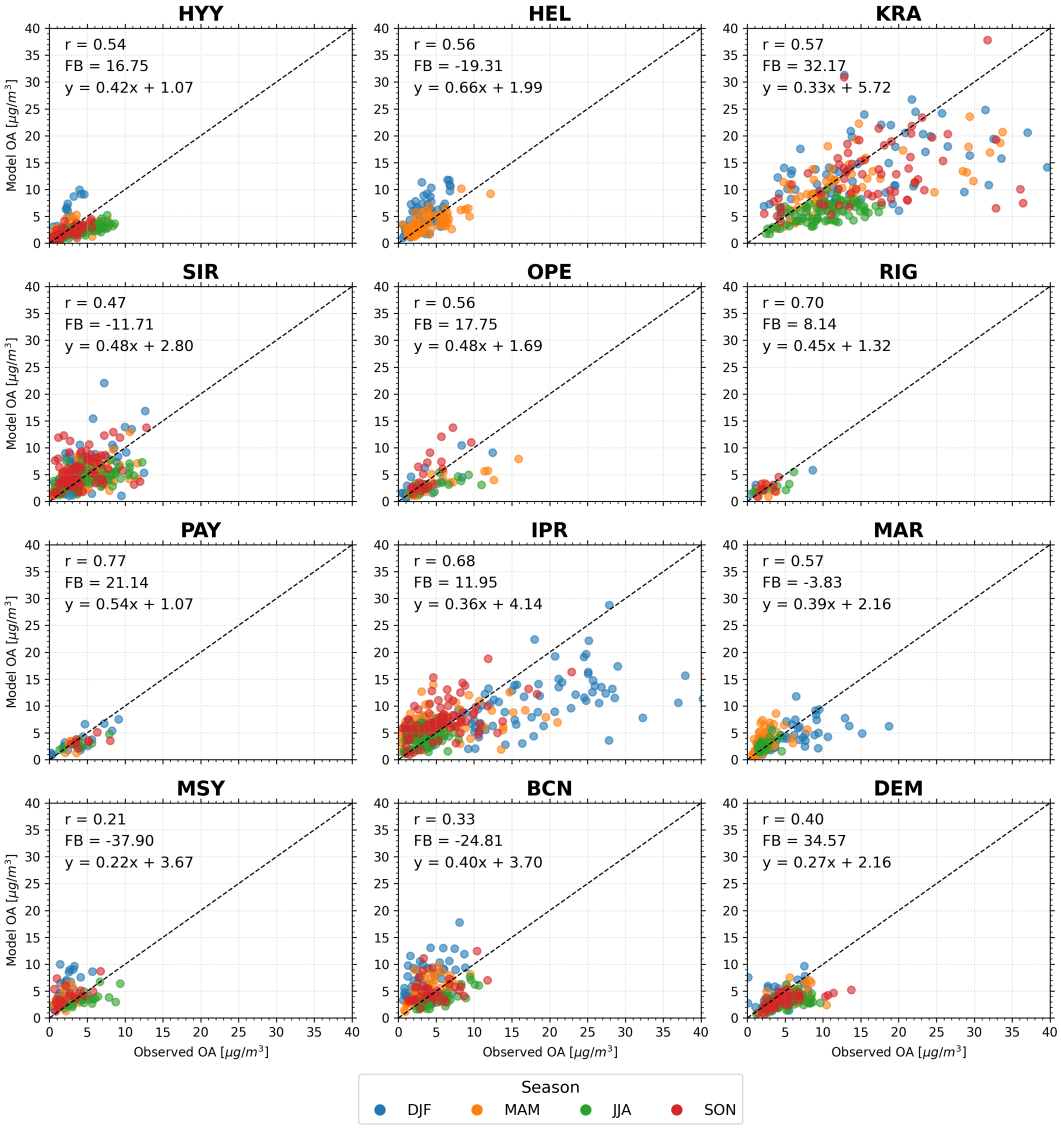

Figure S2. Scatter plots comparing modeled and observed OA concentrations across twelve different locations (HYY, HEL, KRA, SIR, OPE, RIG, PAY, IPR, MAR, MSY, BCN, DEM). Each plot includes data points color-coded by season: DJF (blue), MAM (orange), JJA (green), and SON (red). The plots also display the correlation coefficient (r), fractional bias (FB), and the linear regression equation (y) for each location. The dashed line represents the 1:1 line, indicating perfect agreement between modeled and observed values.

Statistical metrics

Table S1. Statistical metrics used for model performance evaluation. m: model, o: observations.

Metric	Equation	Goal		Criteria	
		OC	EC	OC	EC
Normalized mean bias (NMB)	$\frac{\sum(m_i-o_i)}{\sum o_i} \times 100$	$< \pm 15\%$	$< \pm 20\%$	$< \pm 50\%$	$< \pm 40\%$
Normalized mean error (NME)	$\frac{\sum\lvert m_i-o_i\rvert}{\sum o_i} \times 100$	$< 45\%$	$< 50\%$	$< 65\%$	$< 75\%$
Fractional bias (FB)	$\frac{2}{N}\sum \frac{(m_i-o_i)}{(o_i+o_i)}$	$< \pm 30\%$[a]	$< \pm 30\%$[a]	$< \pm 60\%$[a]	$< \pm 60\%$[a]
Factor two (FAC2)	Fraction where $0.5 < m/o < 2$	–	–	$\geq \pm 50\%$[b]	$\geq \pm 50\%$[b]
Pearson correlation coefficient (r)	$\frac{\sum[(m_i-\overline{m})\times(o_i-\overline{o})]}{\sqrt{\sum(m_i-\overline{m})^2\times\sum(o_i+\overline{o})^2}}$	–	–	–	–
Bias	$\frac{\sum(m_i-o_i)}{N}$	–	–	–	–
Root mean square error (RMSE)	$\sqrt{\frac{1}{N}\sum(m_i-o_i)^2}$	–	–	–	–

[a] Recommended FB values for PM by Boylan and Russell (2006).
[b] Recommended metrics for air quality models by Chang and Hanna (2004) and Soni et al. (2021).

Statistical evaluation for all cases

Table S2. Statistical evaluation of absorption results for Cases 1 to 5.

Cases	Case 1			Case 2			Case 3			Case 4			Case 5		
Metric	r	FB	FAC2	r	FB	FAC2	r	FB	FAC2	r	FB	FAC2	r	FB	FAC2
HYY	0.34	16.06	63.60	0.34	17.63	63.96	0.36	18.84	63.25	0.34	16.65	63.96	0.28	-6.66	58.66
HEL	0.55	10.48	73.42	0.54	10.11	73.15	0.55	9.39	73.42	0.54	11.56	74.79	0.48	20.22	78.08
KRA	0.57	-103.14	49.28	0.57	-103.09	49.28	0.56	-101.11	48.92	0.57	-102.97	48.92	0.51	-103.73	43.17
SIR	0.74	-18.44	71.90	0.74	-19.00	71.63	0.74	-17.23	70.80	0.74	-17.59	71.07	0.62	-44.08	56.75
OPE	0.73	9.85	83.17	0.73	10.19	82.85	0.70	14.22	80.58	0.72	11.80	80.58	0.41	-27.71	56.31
RIG	0.48	-35.39	67.04	0.48	-33.18	65.36	0.49	-32.44	65.08	0.48	-35.53	67.04	0.48	-36.03	67.32
PAY	0.63	-10.27	69.04	0.63	-10.23	69.04	0.63	-10.21	68.77	0.63	-9.77	68.77	0.33	19.11	44.11
IPR	0.72	-28.11	54.40	0.72	-28.06	54.40	0.72	-29.47	53.85	0.72	-28.29	54.40	0.65	-65.44	43.13
MAR	0.55	-16.10	79.04	0.55	-15.75	79.04	0.55	-15.75	79.04	0.55	-15.10	79.32	0.43	-18.21	65.16
MSY	0.53	-11.22	77.78	0.49	49.85	55.84	0.51	52.94	53.56	0.54	-11.64	78.63	0.52	-29.95	80.34
BCN	0.57	28.66	78.68	0.57	28.71	78.68	0.58	28.67	78.68	0.57	29.28	77.94	0.57	26.56	80.88
DEM	0.70	-24.29	84.81	0.70	-24.01	84.45	0.66	-22.70	84.10	0.70	-24.71	84.45	0.49	-60.60	62.54

References

Boylan, J. W. and Russell, A. G.: PM and light extinction model performance metrics, goals, and criteria for three-dimensional air quality models, Atmospheric environment, 40, 4946–4959, 2006.

Chang, J. C. and Hanna, S. R.: Air quality model performance evaluation, Meteorology and Atmospheric Physics, 87, 167–196, 2004.

Guevara, M., Tena, C., Porquet, M., Jorba, O., and Pérez García-Pando, C.: HERMESv3, a stand-alone multi-scale atmospheric emission modelling framework–Part 2: The bottom–up module, Geoscientific Model Development (GMD), 13, 873–903, 2020.

Navarro-Barboza, H., Pandolfi, M., Guevara, M., Enciso, S., Tena, C., Via, M., Yus-Díez, J., Reche, C., Pérez, N., Alastuey, A., et al.: Uncertainties in source allocation of carbonaceous aerosols in a Mediterranean region, Environment international, 183, 108 252, 2024.

Soni, A., Mandariya, A. K., Rajeev, P., Izhar, S., Singh, G. K., Choudhary, V., Qadri, A. M., Gupta, A. D., Singh, A. K., and Gupta, T.: Multiple site ground-based evaluation of carbonaceous aerosol mass concentrations retrieved from CAMS and MERRA-2 over the Indo-Gangetic Plain, Environmental Science: Atmospheres, 1, 577–590, 2021.